CHEMISTRY OF MATERIALS

pubs.acs.org/cm Article

Superconductivity on a Bi Square Net in LiBi

Karolina Górnicka, Sylwia Gutowska, Michał J. Winiarski, Bartlomiej Wiendlocha, Weiwei Xie, R. J. Cava, and Tomasz Klimczuk*

Cite This: *Chem. Mater.* 2020, 32, 3150–3159

Read Online

ACCESS | Metrics & More | Article Recommendations | Supporting Information

ABSTRACT: We present the crystallographic analysis, superconducting characterization and theoretical modeling of LiBi, that contains the lightest and the heaviest nonradioactive metal. The compound crystallizes in a tetragonal (CuAu-type) crystal structure with Bi square nets separated by Li planes (parameters a = 3.3636(1) Å and c = 4.2459(2) Å, c/a = 1.26). Superconducting state was studied in detail by magnetic susceptibility and heat capacity measurements. The results reveal that LiBi is a moderately coupled type-I superconductor ($\lambda_{e\text{-}p}$ = 0.66) with T_c = 2.48 K and a thermodynamic critical field $H_c(0)$ = 157 Oe. Theoretical studies show that bismuth square net is responsible for superconductivity in this compound, but the coupling between the Li planes and Bi planes makes a significant contribution to the superconductivity.

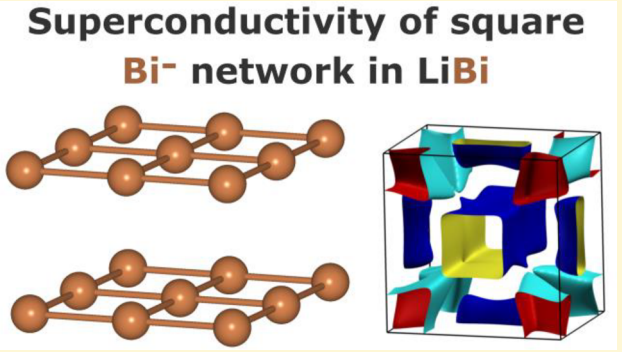

INTRODUCTION

The two-dimensional electronic structures of square nets are an important current topic in materials physics.[1,2] A net of this geometry is present in high temperature copper and iron based superconductors and is responsible for their high temperature transition to the superconducting state. In addition, compounds with a Bi square net are of great current interest due to their importance in topological physics and are extensively studied by both theorists and experimentalists.

Bismuth is the heaviest nonradioactive element, and is widely used in solid state laboratories around the world. In contrast to its neighbors in the periodic table (Pb and Po), Bi is nontoxic and can be treated as nonradioactive (though it actually has a half-life 1.9×10^{19} years,[3] a billion times longer than the age of the universe). What is special about Bi from our perspective is its electronic configuration in charge-transfer-based compounds, it can commonly be present as a cation, that is, as Bi^{3+} ($6s^26p^0$) or Bi^{5+} ($6s^06p^0$), or an anion, that is, as Bi^{3-} ($6s^26p^6$). Formal oxidation states of −1 and −2 are also observed, often forming a square net in compounds that reveal novel electronic behavior, such as superconductivity. Superconductivity in layered compounds with Bi square nets has been reported for $CeNi_{0.8}Bi_2$,[4] $LaPd_{1-x}Bi_2$,[5] $SrMnBi_2$[6] Y_2O_2Bi,[7] and $CaBi_2$.[8]

The elemental antipode to bismuth in the periodic table, the first and lightest metal known is lithium. Found in the upper left corner of the periodic table with a single valence electron, Li is a highly a reactive metal, with a strong tendency to donate electrons. Lithium-based compounds are often unstable in air and hence frequently require special attention during synthesis and characterization. Reacting the lightest and the heaviest metals together in a 1:1 ratio, one gets the LiBi binary compound. Surprisingly, it does not form in the CsCl structure type, common for many intermetallic compounds.[9] Instead it forms in a tetragonal (CuAu-type) crystal structure with c/a = 1.26.[10] For the next metal down the alkali column in the periodic table, Na, the analogous NaBi compound also forms in the same basic structure, although the distortion is larger, with c/a = 1.39.[11] Proceeding further down the column, KBi crystallizes in a more complex structure, featuring infinite Bi–Bi spirals, closely resembling the Te–Te chains observed in elemental tellurium.[12]

LiBi has previously been reported as a superconductor, but except for T_c and its pressure derivative[13] and the Li isotope effect,[14] no more information concerning its normal and superconducting states is available. Here we describe our experimental and theoretical studies of LiBi. We show that LiBi is a type-I superconductor and that the superconductivity is purely driven by electrons on the formally Bi^{1-} square net. The relevance of the structural distortion of LiBi from ideal cubic to observed tetragonal symmetry to the superconductivity is proposed.

Received: January 15, 2020
Revised: March 15, 2020
Published: March 16, 2020

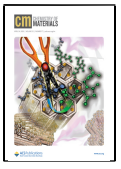

https://dx.doi.org/10.1021/acs.chemmater.0c00179
Chem. Mater. 2020, 32, 3150–3159

RESULTS AND DISCUSSION

Single crystals of LiBi were grown by the flux method, using a Bi flux. The obtained crystals show plate-like shape and metallic luster. The typical SEM image of the as-grown LiBi single crystal is presented in Figure 1 in the Supporting Information (SI). The purity and crystallographic structure of crushed crystals was tested by powder X-ray diffraction (see SI). All the Bragg lines can be indexed to the tetragonal crystal structure of LiBi, with centrosymmetric space group *P4/mmm* (No. 123), plus elemental Bi (remaining flux or decomposition product) present as impurity. The sharpness of diffraction peaks reflects the good crystallinity of the sample. A LeBail fit to the diffraction pattern yields the lattice parameters a = 3.3636(1) Å and c = 4.2459(2) Å, in good agreement with the previously reported values.[10] Additional pXRD scans were performed on a pulverized sample exposed to air for 2 and 12 h. Although the patterns showed that the LiBi phase is stable after 2 h in air, the compound completely decomposes after the longer time period, with only Bi reflections observed.

Low-temperature α-LiBi has a tetragonal CuAu-type crystal structure[15,16] which can be viewed as variant of the cubic *Pm-3m* CsCl-type structure elongated along the z axis (see Figure 1(a)). Such a structure is difficult to understand in the simple framework of dense packing of hard spheres, which should lead to a CsCl- or NaCl-type structure. Moreover, in the isoelectronic compounds such as KBi, NaSb, and LiAs, one-dimensional spirals of pnictogen atoms are found instead of the square network. The occurrence of these spirals can be understood in the framework of the Zintl–Klemm concept: with a single electron transfer from K, Bi acquires a formal electron configuration of Bi^- [Xe] $6s^2$ $6p^4$ and becomes isoelectronic with chalcogens which, in case of heavier members (Se, Te), feature infinite 1D chains similar to the ones observed in KBi, as well as in NaSb and LiAs. These chains can be derived from a simple cubic arrangement of pnictogen atoms by a distortion that breaks four of the six bonds between nearest-neighbors. From the viewpoint of the VSEPR theory these 1D spirals suggest the presence of two sp^3 lone pairs on each Bi^-, resulting in a bent-linear geometry of each (Bi–Bi–Bi) unit (the local coordination of Bi^- is distorted tetrahedral due to lone pair repulsion being stronger than the tendency to form bonding pairs).

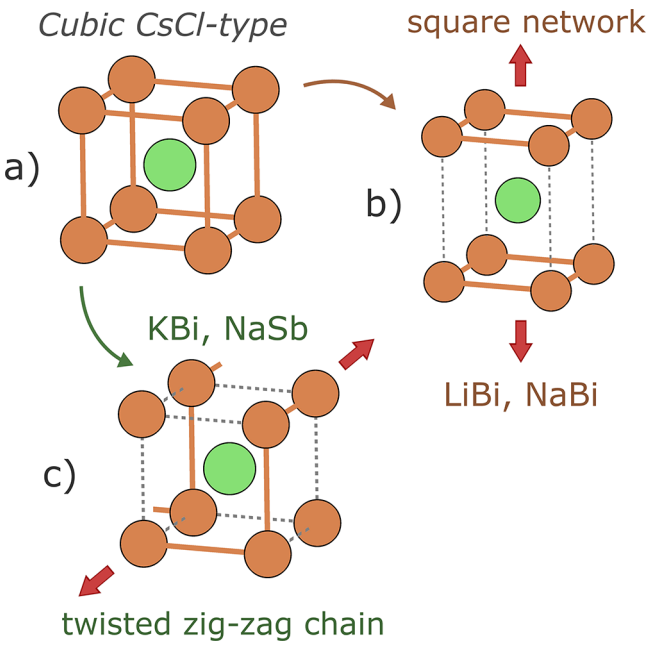

Figure 1. In the hypothetical cubic CsCl-type LiBi, each Bi atom forms six close contacts with neighboring Bi. As discussed in the manuscript, the structure is unstable toward a distortion either to a variant featuring planar Bi square networks (seen in room-temperature structures of LiBi and NaBi) (b) or a twisted zigzag chain arrangement (c) found, e.g., in KBi and NaSb, which also resemble chains found in elemental tellurium. Both (b) and (c) variants can be derived from the cubic parent by selectively breaking 2 or 4 bonds at each Bi site, respectively.

Having the same electron count as KBi, LiBi (and isostructural NaBi) should also form these spiral chains and become semiconducting. Instead, we observe perfect square framework of Bi^-, which results from breaking only two of the six possible bonds, leaving a four-connected network. As pointed out by Papoian and Hoffmann,[2] a square network with ns^2 np^4 species (as Sb^- or Bi^-) is unstable toward at least three types of distortion, one of them being the formation of zigzag chains. Nesper suggested that the structure of LiBi is stabilized by relativistic effects, namely (a) the contraction of s orbitals,[2,17] which reduces the s-p overlap and leaves only p valence orbitals available for bonding (note that good s-p overlap is necessary to produce sp^3 hybrid atomic orbitals and a locally tetrahedral coordination), and (b) the spin–orbit splitting of triply degenerate p orbitals into nondegenerate $p_{1/2}$ and doubly degenerate $p_{3/2}$, the former being significantly lower in energy. With six electrons per Bi, this results in s and $p_{1/2}$ bands being completely filled, leaving two electrons for two $p_{3/2}$ orbitals that available for forming Bi–Bi bonds.

From the viewpoint of our electronic structure calculations, presented in the last part of the paper, this stabilization of the square Bi network can be at least partially attributed to the effects of spin–orbit coupling that strongly affects the shape of Fermi surface (FS), weakening the possible FS nesting. Such an effect was previously postulated to be responsible for stabilization of the simple cubic structure of Po with respect to the trigonal structure of the isoelectronic elemental Te.[18] On the other hand, Tremel and Hoffman[1] have shown that in case of the isoelectronic compounds $EuSb_2$ and $YbSb_2$ the stabilization of the Sb square network in the latter stems from the small contribution of trivalent Yb in contrast to the purely divalent character of Eu in the former. This also implies that the effect is caused by a stronger covalent character of Yb–Sb bonding, in agreement with the electronegativity differences (Eu: 1.01 vs Yb 1.06). The same reasoning can be applied to the LiBi-NaBi-KBi and NaBi-NaSb-NaAs series, as K is more electropositive than both Li and Na, whereas both Sb and As are more electronegative than Bi, resulting in a more "ionic" bonding, leading to a Peierls distortion, formation of spiral pnictogen polyanions, and opening of the band gap, in agreement with the Zintl picture.

A high-temperature β- phase has been reported for LiBi, but its structure has not been established due to its very narrow temperature stability range.[15] From simple entropic reasoning, one may expect that the β–α transformation on cooling is a symmetry-breaking transition, and the likely higher-symmetry variant of the CuAu-type structure is a cubic CsCl-type lattice with a simple cubic arrangement of Bi atoms. The related LiPb compound is known to undergo a symmetry breaking transition around 200 °C from CsCl-type cubic structure to a trigonally distorted (elongated along the (111) axis) $R\bar{3}m$

https://dx.doi.org/10.1021/acs.chemmater.0c00179
Chem. Mater. 2020, 32, 3150–3159

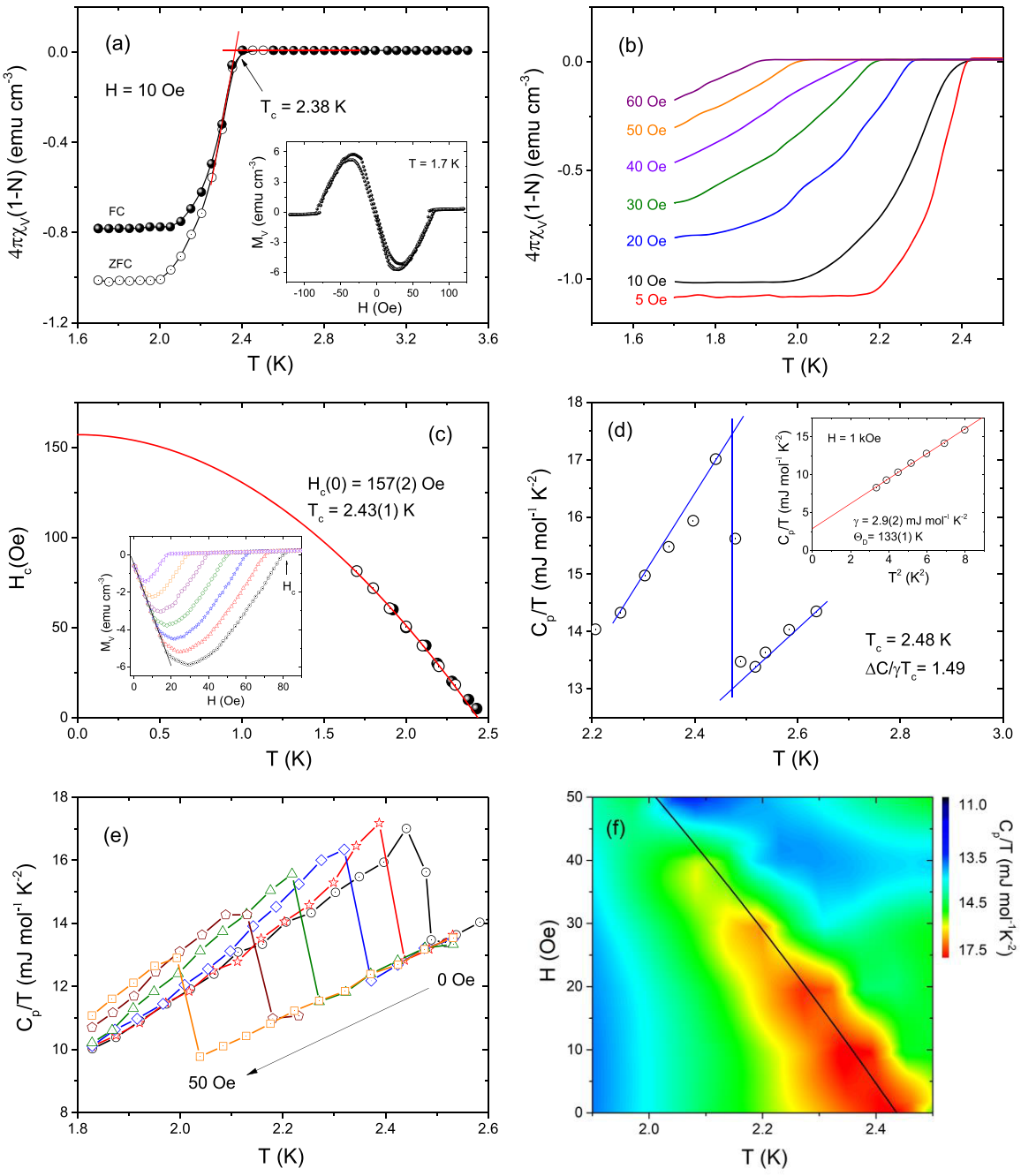

Figure 2. (a) The main panel shows zero-field-cooled (ZFC) and field-cooled (FC) temperature-dependent volume magnetic susceptibility $\chi_V(T)$ measurements performed under a small applied magnetic field of 10 Oe. The inset presents a full magnetization loop measured at T = 1.7 K. (b) The temperature-dependent volume magnetic susceptibility in several different magnetic fields. (c) Main panel: The temperature variation of the thermodynamic critical field (H_c). Inset: volume magnetization, M_V, vs applied field at various temperatures from 1.7 to 2.3 K. (d) The specific heat anomaly in zero magnetic field at low temperatures with T_c = 2.48 K. Inset: C_p/T vs T^2 measured at 1 kOe. A red solid line represents a linear fit used to estimate the values of electronic and phonon specific heat coefficients. (e) The dependence of the specific heat C_p on temperature in applied magnetic fields H up to 50 Oe. (f) Map of the specific heat of LiBi as a function of temperature and applied magnetic field.

structure.[15,16,19] LiPb has one valence electron less than LiBi, and one can expect that the bonding will be stronger as the population of antibonding states is lower. In fact the Pb−Pb distance is of the order of 3.60 Å in both high- and low-temperature phase,[16,19] shorter than the average value $\frac{2a+c}{3}$ = 3.66 Å in α-LiBi.

As was proposed earlier for SrSnP and NbRuB,[20,21] a superconducting transition is one of the possible ways (besides a structural distortion or a magnetic transition) of reducing the total energy of an electronic system, which is larger when the valence electrons are in antibonding orbitals. The superconducting state for LiBi was initially characterized via measurements of its magnetic properties. The temperature-dependent volume magnetic susceptibility χ_V(T) in a small applied field of 10 Oe is shown in Figure 2(a). Both zero-field-cooled (open circles) and field-cooled (full circles) data show a sharp diamagnetic transition at T_c = 2.38 K, reflecting the

https://dx.doi.org/10.1021/acs.chemmater.0c00179
Chem. Mater. 2020, 32, 3150−3159

Table 1. Estimated and calculated parameters of LiBi and NaBi.[26]

		calculations				experiment	
parameter	unit	LiBi w/o SOC	LiBi w. SOC	NaBi w.SOC	Li^6Bi	LiBi	NaBi
$DOS(E_F)$	eV^{-1}/f.u	0.68	0.67	0.61		0.74	0.88
γ	mJ mol^{-1} K^{-2}	1.59	1.59	1.53		2.90	3.4
$\lambda_{e\text{-}p}= \gamma_{expt}/\gamma_{calc} -1$		0.82	0.82	1.36			
$\lambda_{e\text{-}p}(\alpha^2F/McMillan)$		0.61[a]	0.66[a]	0.62[a]	0.66[a]	0.66[b]	0.62[b]
ω_{log}	K	90.2	86.4	71.5	87.3		
T_c (α^2F, μ = 0.11)	K	2.06	2.48	1.67	2.51	2.48	2.15
T_c (α^2F, μ = 0.13)	K	1.63	2.03	1.33	2.05		
Θ_D	K					133	140
$\Delta C_p/\gamma T_c$						1.49	0.78

[a]From the computed Eliashberg function α^2F. [b]From the inverted McMillan formula.

occurrence of superconductivity in this material. The superconducting critical temperature, T_c, is conservatively estimated as being the intersection between the line obtained by extrapolation of the normal-state magnetic susceptibility to lower temperatures and the steepest slope line of the diamagnetic superconducting signal. The estimated value of T_c = 2.38 K is in very good agreement with the value reported previously by Sambongi.[14] After taking into account the demagnetization effect of the sample by using the formula $-4\pi\chi_V = 1/(1 - N)$, where N = 0.75 is the demagnetization factor (obtained from the M(H) fit discussed next), the superconducting volume fraction estimated from the zero-field-cooled dc susceptibility is close to 100%, a signature of the bulk superconductivity in LiBi. The relatively small difference between the FC and ZFC magnetic susceptibility is due to the character of the tested sample, for which flux pinning is weak. A full magnetization loop measured at T = 1.7 K is shown in the inset of Figure 2(a). The M(H) curve initially shows a linear dependence on the magnetic field, and then drops to zero near the critical field. This is a characteristic feature of type-I superconductors, such as YSb_2,[22] KBi_2,[23] $ScGa_3$, $LuGa_3$,[24] and $ReAl_6$.[25] The broadening of the M(H) data from a pure sawtooth is likely a consequence of demagnetization effects.

Figure 2(b) shows the temperature-dependent volume magnetic susceptibility in several different magnetic fields, H = 5, 10, 20, 30, 40, 50, and 60 Oe. With increasing H, the width of the superconducting transition increases slightly and T_c systematically shifts to lower temperature. Defining the critical temperature as the onset of diamagnetic ZFC susceptibility for each field, the values obtained were then used to determine the thermodynamic critical field H_c (see the main panel of Figure 2(c)). The inset in Figure 2(c) presents the low-field parts of the dc magnetization isotherms measured at various temperatures (from 1.7 to 2.3 K). Assuming that the initial response to magnetic field is perfectly diamagnetic, the demagnetization factor N = 0.75 was found, consistent with the sample's shape used in the magnetic measurements. The critical fields were extracted for each temperature as being where the material enters the normal state. Using these data, the temperature variation of the thermodynamic critical field is shown in the main panel of Figure 2(c). The data points shown as full circles are extracted from the $\chi_V(T)$ analysis and the open circles are obtained from the $M_V(H)$ measurements. The data points thus obtained were analyzed with the following formula:

$$H_c(T) = H_c(0)\left[1 - \left(\frac{T}{T_c}\right)^2\right] \quad (1)$$

where $H_c(0)$ is the critical field at 0 K and T_c is the superconducting critical temperature. The fit (solid red line) is very good and yields T_c = 2.43(1) K and $H_c(0)$ = 157(2) Oe. The critical temperature obtained from this analysis is very close to the T_c obtained from the magnetic susceptibility measurements.

Further information on the superconducting transition of LiBi can be gained from specific-heat measurements. The results of low-temperature heat capacity measurements are shown in Figure 2(d). The zero-field data of LiBi are plotted as C_p/T versus T. The bulk superconductivity in LiBi is manifested by the pronounced anomaly in the specific heat data. From the graphical equal-area construction (blue solid lines), which reflects the expected entropy balance between the normal and the superconducting states at the superconducting phase transition, the estimated critical temperature is equal to 2.48 K, consistent with the value determined from magnetic susceptibility measurements. The specific heat jump at T_c is found to be $\Delta C/T_c$ = 4.3 mJ $mol^{-1}K^{-2}$.

The inset in Figure 2(d) presents the variation in C_p/T with T^2 at under magnetic field of 1 kOe, which is above H_c; thus the material is in its nonsuperconducting state. The specific heat data provide an extrapolation of the normal-state behavior to $T \rightarrow 0$ and allow the determination of the Sommerfeld coefficient γ from the equation $C_p/T = \gamma + \beta T^2$, where the second term is the phonon contribution to the specific heat. The fit, represented by the red solid line, gives γ = 2.9(2) mJ $mol^{-1}K^{-2}$ and β = 1.64(4) mJ $mol^{-1}K^{-4}$. Furthermore, the Debye temperature Θ_D can be determined using the simple Debye model:

$$\Theta_D = \left(\frac{12\pi^4}{5\beta}nR\right)^{1/3} \quad (2)$$

where R = 8.31 J $mol^{-1}K^{-1}$ and n = 2 for LiBi. Using β = 1.64(4) mJ $mol^{-1}K^{-4}$, the calculated Debye temperature is 133(1) K, comparable with Θ_D = 140 K reported for NaBi.[26] With the estimated Debye temperature Θ_D in hand, the electron−phonon coupling constant, $\lambda_{e\text{-}p}$, can be then estimated from McMillan's theory[27] as

$$\lambda_{e-p} = \frac{1.04 + \mu^*\ln(\Theta_D/1.45T_c)}{(1 - 0.62\mu^*)\ln(\Theta_D/1.45T_c) - 1.04} \quad (3)$$

https://dx.doi.org/10.1021/acs.chemmater.0c00179
Chem. Mater. 2020, 32, 3150−3159

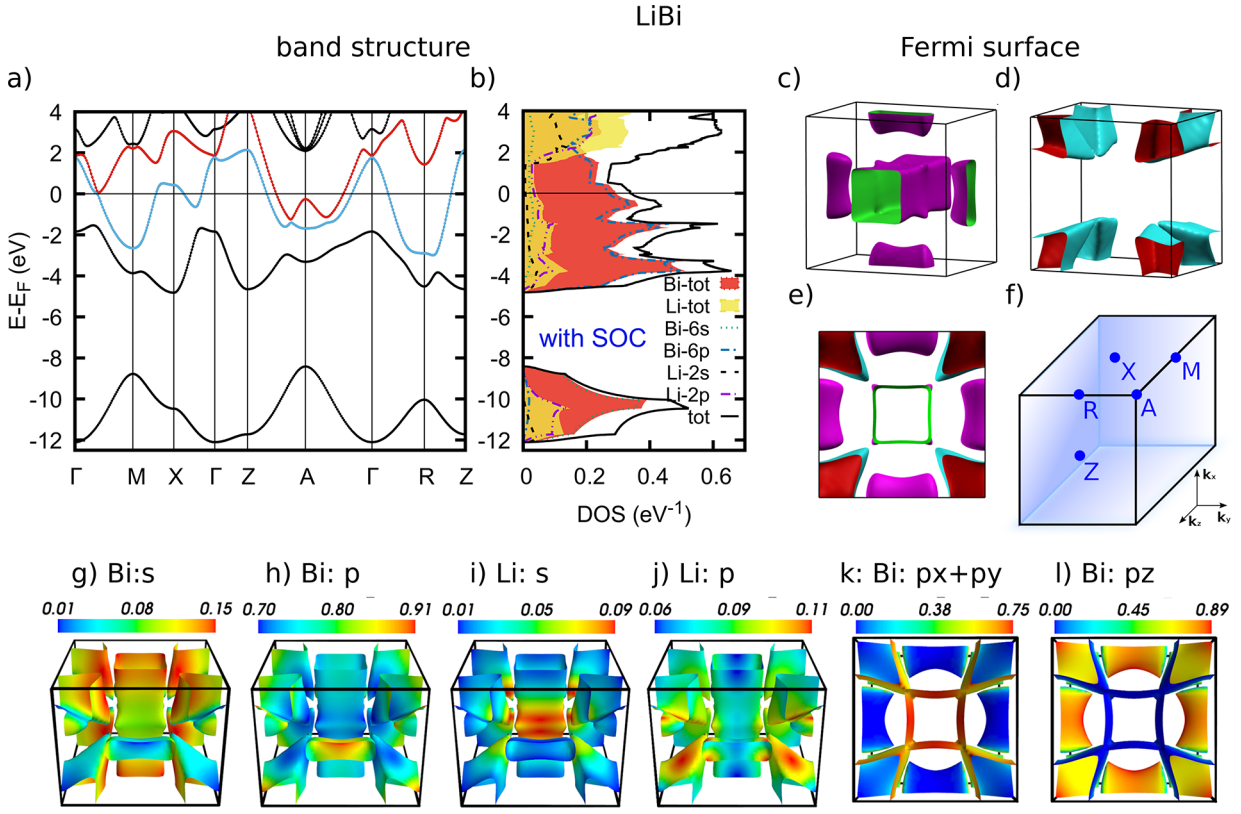

Figure 3. Electronic structure of LiBi in terms of (a) band structure, (b) DOS (with partial DOS coming from atoms and from orbitals marked as a filled curve and colored lines respectively), and (c–e) the Fermi surface calculated with SOC. Brillouin zone (f) is also attached. Atomic orbital character of the Fermi surface of LiBi calculated with SOC are presented in panels g–j calculated with SOC, while the projections into the nonrelativistic p_x, p_y, and p_z basis (calculated without SOC), are presented in panels k,l. The p states of Bismuth are crucial in the electronic structure of LiBi around the Fermi level and are only slightly hybridized with s states.

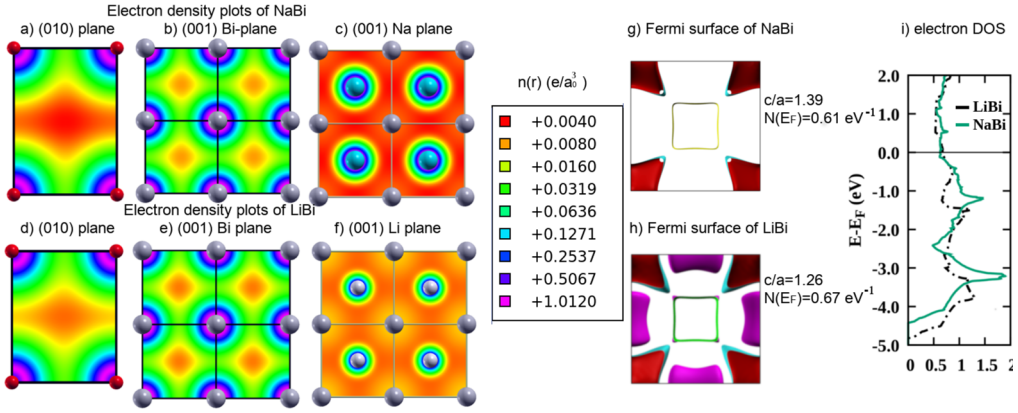

Figure 4. Comparison of LiBi and NaBi compounds in terms of (a–f) electron density, (g–h) Fermi surface, and (i) electron DOS. Due to smaller distortion in LiBi, Bismuth planes and Li atoms are less separated, which contributes to the stronger electron–phonon coupling and T_c, comparing to NaBi.

where, μ^* is the repulsive screened Coulomb parameter, usually taken as $\mu^* = 0.13$ for intermetallic superconductors.[28−30] Taking $T_c = 2.48$ K and $\Theta_D = 133$ K, the calculated $\lambda_{e\text{-}p}$ is 0.66, implying that LiBi is weakly or moderately coupled BCS superconductor.

Using the Sommerfeld coefficient $\gamma = 2.9(2)$ mJ mol^{-1}K^{-2} and the value of the specific heat jump at T_c ($\Delta C/T_c = 4.3$ mJ mol^{-1}K^{-2}), the ratio $\Delta C/\gamma T_c$ can be calculated. The normalized specific heat jump is equal to 1.49, which is near to the expected value of 1.43 for a weakly coupled BCS superconductor.

As shown in Figure 2(e), field-dependent specific heat measurements were performed in fields up to 50 Oe. As expected, the jump in specific heat at $H = 10$ Oe (the lowest applied H) is higher and sharper than that at zero magnetic field, indicating a crossover from second- to the first-order phase transition, commonly seen in type-I superconductors.[23,31,32] The panel of Figure 2(f) presents a map of the specific heat of LiBi as a function of temperature and applied magnetic field (up to 50 Oe) in the vicinity of the superconducting transition. The black solid fit line to eq 1 is shown in a main panel of Figure 2(c) and confirms the

https://dx.doi.org/10.1021/acs.chemmater.0c00179
Chem. Mater. 2020, 32, 3150−3159

complementarity of both experimental methods employed. This is the borderline between normal and superconducting states. The estimated superconducting and normal state parameters of LiBi are gathered in Table 1. Our analysis suggests weak-coupling type - I superconductivity for LiBi.

We now discuss the electronic structure of LiBi and compare it to NaBi. Figure 3 presents the calculated electronic band structure of LiBi in terms of its dispersion relations, DOS and Fermi surface. Spin−orbit coupling (SOC) is included in calculations. Additionally, Figures 3(g−j) show the atomic orbital character of the Fermi surface calculated as a projection of the wave function onto atomic wave functions. The split of the Bi p-orbital into $p_x + p_y$ and p_z shown at Figure 3(k,l) is calculated without SOC, as such designations correspond to a nonrelativistic basis. In Figure 4 the charge density plot, the Fermi surface and the DOS are presented and compared to the same characteristics of NaBi. As the charge density plots (see Figure 4(a)) show, due to the distortion from the cubic to the tetragonal structure along the [001] axis, the bismuth atoms in both materials form metallic layers that are separated from each other. This is reflected in the shape of Fermi surface as well as in the filling of the p orbitals, as shown below.

Atomic Bi has 6p and 6s orbitals occupied by three and two valence electrons respectively, for a total of five, while in the case of the alkali Li, one electron occupies an s-orbital and the p-orbital is empty. This gives six electrons per f.u. for the LiBi crystal. Bi is more electronegative than Li, thus we expect the transfer of the electron from the s-orbital of Li to Bi. This is reflected quantitatively in the calculations. The Bader analysis, performed with help of Critic2 software,[33] indeed indicates that 0.85e of charge is transferred from the Li atom to the Bi atom in LiBi. As shown in Figure 3(a), in the energy range from −12 to −8 eV below E_F there is a semicore hybridized sp band dominated by the 6s state of Bi with the contribution of 2p states of Li. The main valence band block spans the range between −5 eV and E_F, and consists of one completely filled and two partially filled bands. Figure 3(b) shows these bands to be dominated by the 6p states of Bi hybridized with the 2s and 2p states of Li.

The resulting Fermi surface consists of two pieces, as is shown in Figure 3(c,d). Figure 3(e) presents the [001] view of the Fermi surface. The hole-like band, marked in Figure 3(a) with the blue line, is connected with the first piece of Fermi surface (Figure 3(c)), which consists of pockets centered at the X point and the cuboid-like part. The electron-like band, marked with the red line in Figure 3(a), is connected to second piece of FS (Figure 3(d)), consisting of pockets centered at the A-points. The cuboid-like part of Fermi surface is open in the k_z direction, which is a signature of the quasi-two-dimensional character for this sheet. As shown in Figure 3(g−l), parts of the Fermi surface parallel to the [001] axis, including the cuboid-like part, come from the p_x and p_y states of Bi hybridized with the s-states of Li and Bi, while the parts in the (001) plane have p_z character hybridized with the p-states of Li. This stands in agreement with the charge density plots, which show bismuth layers to be metallic and separated from each other. These calculations show that the square Bi planes have a k-space signature.

The results of scalar-relativistic calculations (i.e., neglecting SOC) are shown in the SI. Comparison with relativistic results shows that SOC strongly modifies electronic structure of LiBi, as expected for a Bicontaining compound. This influence, however, is not in the vicinity of the Fermi level. Thus, the calculations ignoring the SOC and including the SOC lead to almost the same Fermi surface shape and DOS (E_F) values (0.68 eV^{-1} versus 0.67 eV^{-1}, see Table 1).

There are many similarities between the electronic structures of LiBi and NaBi,[26,34] which superconducts at a T_c = 2.15 K. The electronic structures of these compounds are compared in Figure 4. The DOS at E_F (our calculated values are 0.61 eV^{-1}/f.u for NaBi and 0.67 eV^{-1}/f.u for LiBi) and the electron−phonon coupling parameters are similar. The differences are as follows. First of all, the structural distortion along the [001] direction is bigger in case of NaBi (c/a = 1.39) than in LiBi (c/a = 1.26). This fact is reflected in the charge density plots, where the Bismuth layers are more separated from each other (see Figure 4(a)) than in LiBi (see Figure 4(d)). Because of that, the pockets around X point found in the Fermi surface (see Figure 4(h)) of LiBi disappear in NaBi (see Figure 4(g)), which is reflected in a slightly smaller value of DOS at Fermi level in NaBi (Figure 4(i)). Moreover, the charge density in the plane of sodium (Figure 4(c)) is smaller than in the plane of lithium (Figure 4(f)), while atomic plane of bismuth is metallic-like in both cases (Figure 4(b,e)), thus it cannot be an effect of a slightly bigger lattice parameter in the case of NaBi (a = 3.41 Å) in comparison to LiBi (a = 3.37 Å), it may rather be a consequence of the smaller electronegativity of sodium. Thus, the electrons may be more intensively transferred to bismuth in the case of NaBi than in LiBi. Thus, there is a lower electronic density around sodium than around lithium, which is important for the electron−phonon coupling, as discussed below.

Besides superconductivity, topological surface states have been suggested to exist in NaBi.[34] The analysis of the topological properties in ref 34 has been performed using the Z2 invariant, however, which is not well-defined in a three-dimensional metallic case where no band gap is present. In the current material, therefore, due to the absence of a band gap in any of the planes in the Brillouin zone, even weak topological insulating properties are not expected.

Our calculated phonon dispersion relations, with phonon line widths $\gamma_{q\nu}$ marked at each wave vector q and phonon branch ν, the density of states $F(\omega)$ decomposed into atomic contributions, and the Eliashberg electron−phonon coupling function $\alpha^2F(\omega)$, decomposed over phonon modes, are shown in Figure 5. As there are two atoms in the unit cell of LiBi, six phonon branches, three acoustic and three optic, are seen. Due

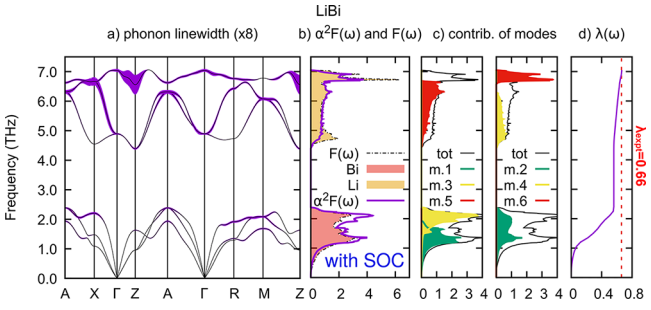

Figure 5. Phonons and electron−phonon coupling of LiBi shown in terms of (a) phonon dispersion relation with phonon line width marked as a fatband, (b) phonon DOS decomposed into atomic contribution marked as a filled curve and Eliashberg function $\alpha^2F(\omega)$ normalized to phonon dos, (c) partial $\alpha^2F_n(\omega)$ where n runs over phonon modes and (d) the cumulative electron−phonon coupling constant λ_{e-p}.

https://dx.doi.org/10.1021/acs.chemmater.0c00179
Chem. Mater. 2020, 32, 3150−3159

to the huge mass difference ($m_{Bi} \simeq 30m_{Li}$), the low-frequency part arises mostly from Bi and the optic part from Li vibrations. These two groups of phonon modes are well separated: the acoustic part has calculated frequencies in the range from 0 to 2.5 THz, while the optic modes are found between 4.5 and 7 THz. Both these ranges, as well as the gap between them, are much bigger than in the case of NaBi[34] (0 to 2 THz for the acoustic and 2.25 to 5 THz for the optic modes, respectively). Our computational results for NaBi are presented in the SI.

The increase of Li frequencies with respect to Na frequencies is in agreement with a simple diatomic chain model. Having the chain of two types of atoms: Bi plus Li or Na, one gets the optical frequencies at gamma equal to $\omega_{LiBi} = 2C(m_{Li} + m_{Bi})/(m_{Li}m_{Bi}) = 0.54C$ (C is a constant) in case of LiBi and $\omega_{NaBi} = 0.31C$ in case of NaBi. Its ratio is equal to $\omega_{LiBi}/\omega_{NaBi} = 1.74$. Calculations performed in this work and in ref 34 show the frequency of two (degenerate at gamma) lower optical modes to be $\omega_{LiBi} = 4.89$ THz and $\omega_{NaBi} = 2.79$ THz, which gives the ratio of $\omega_{LiBi}/\omega_{NaBi} = 1.75$ in excellent agreement with the chain model.

These two described optical branches have a considerable dispersion, while the highest optical branch is rather narrow and well-separated from the other branches. As shown in the SI, the fourth and fifth phonons with wave vector $\mathbf{q} = (0,0,0.5)$ (point Z in the Brillouin zone) are associated with the displacement of Li atoms along the [110] direction. The same holds for phonons at the Γ and A points in the Brillouin zone. Since the unit cell is shorter along the [100] and [010] axes in comparison to the [001] axis, in the (001) plane the Li atoms are much closer to each other than in the [001] direction and the Bi−Li and Li−Li distances are nearly equal. This can explain the agreement with predictions of the chain model as well as the considerable dispersion of these two branches. On the other hand, the sixth phonon mode is associated with vibration of atoms along the [001] direction, where the lattice parameter is larger and the atoms are more separated, making the highest phonon mode an Einstein-like less dispersive one.

As far as the electron−phonon interaction is concerned, the largest phonon line width $\gamma_{q\nu}$ (corresponding to the strongest coupling, see ref 35) is observed for the above-mentioned highest frequency optical mode at the Z point. Here both the phonon propagation vector and Li atomic displacement are along the z-axis. This vibration will strongly affect the Bi−Li bonding, and thus a strong effect on the corresponding electronic states is expected. Especially, this may strongly influence the p_z orbitals of Bi, which are essential for the tetragonal distortion of the crystal structure of this compound.

Large phonon line widths contribute to the Eliashberg function $\alpha^2F(\omega)$, which is defined as a sum over all the phonons:

$$\alpha^2F(\omega) = \frac{1}{2\pi N(E_F)} \sum_{q\nu} \delta(\omega - \omega_{q\nu}) \frac{\gamma_{q\nu}}{\hbar\omega_{q\nu}} \quad (4)$$

and which is used to calculate the electron−phonon coupling constant $\lambda_{e-p} = 2\int_0^{\omega_{max}} \frac{\alpha^2F(\omega)}{\omega} d\omega$. However, as one can see $\lambda_{e-p} \propto \frac{\gamma_{q\nu}}{\omega_{q\nu}^2}$, due to this large phonon line width the contribution from this high-frequency branch is important. A total $\lambda_{e-p} = 0.66$ parameter is computed from the Eliashberg coupling function and its frequency distribution, as shown in Figure 5. The acoustic part of the phonon spectrum, dominated by Bi vibrations, contributes about 85% to the total λ_{e-p}, leaving 15% (0.1 in absolute value) for the optic branches.

The Allen-Dynes formula[36]

$$T_c = \frac{\omega_{log}}{1.20} \exp\left[\frac{-1.04(1 + \lambda_{e-p})}{\lambda_{e-p} - \mu^*(1 + 0.62\lambda_{e-p})}\right] \quad (5)$$

is next used to compute the superconducting critical temperature value. As shown in Table 1, $\lambda_{e-p} = 0.66$ results in an experimental value of $T_c = 2.48$ K, when the Coulomb pseudopotential parameter is set to $\mu^* = 0.11$, which confirms that superconductivity in LiBi is accurately described within the electron−phonon mechanism. The calculated value of λ_{e-p} is slightly smaller than extracted from the experimental Sommerfeld parameter with the help of calculated DOS(E_F) value, which is $\lambda_{e-p} = 0.82$ but both values correspond to intermediate coupling regime.

As far as the spin−orbit coupling (SOC) effects are concerned (see SI), in the scalar-relativistic calculations λ_{e-p} is smaller in about 8%, which is caused by the shift of the highest phonon mode to higher frequencies. Thus, in the present case, SOC weakly enhances the electron−phonon interaction strength, in contrast to the recently studied $CaBi_2$ superconductor.[35]

Comparing now the coupling strengths in LiBi and NaBi (see SI for the figures), both λ_{e-p} (0.66 and 0.62 for LiBi and NaBi, respectively) and T_c (2.48 and 2.15 K, respectively) are higher in the case of LiBi. It may seem surprising that the strong hardening in the phonon spectrum of LiBi, resulting in much larger phonon frequency range (0−7.5 THz for LiBi and 0−4.5 THz for NaBi) does not result in the opposite trend, as $\lambda_{e-p} \propto \frac{\gamma_{q\nu}}{\omega_{q\nu}^2}$. In fact, though, this is caused by substantial differences in the Eliashberg function. While in the acoustic part of the spectrum $\alpha^2F(\omega)$ does not differ much between the NaBi and LiBi cases, giving similar (and even slightly larger for NaBi) contribution to the total λ_{e-p} ($\lambda_{e-p}^{acoustic} = 0.56$ in LiBi, $\lambda_{e-p}^{acoustic} = 0.58$ in NaBi), the contribution from the optical branches, especially from the first one, is 2.5 times larger ($\lambda_{e-p}^{optic} = 0.10$ in LiBi, $\lambda_{e-p}^{optic} = 0.04$ in NaBi).

As shown in the SI for the Z-point, where the phonon line widths are the largest in both compounds, the first two degenerate optical modes in LiBi are associated with transverse phonons, where Li atom vibrates in the xy Li−Li plane, while the third one is a longitudal mode along z, where Li vibrates perpendicular to xy Li planes and toward the planes of Bi atoms. In NaBi the same atomic displacements are found. As discussed before, due to the smaller c/a ratio of LiBi and larger electron density around Li, when compared to the Na case, the Li atoms' vibrations couple more effectively to Bismuth electronic states. This gives an additional, though nominally less-expected contribution of the light atom vibrations to the total λ_{e-p} in LiBi compared to NaBi.

In both cases of LiBi and NaBi, the theoretical (calculated from Eliashberg coupling function) and experimental (calculated from McMillan equation) values of λ_{e-p} agree with each other (both equal to 0.66 for LiBi and 0.62 for NaBi), while the values estimated as a renormalization factor of the electronic heat capacity seem to be overestimated (0.82 for LiBi and 1.36 for NaBi). We consider λ_{e-p} obtained from the Eliashberg function and T_c as a more accurate one, and the larger discrepancy observed for NaBi is likely related to

https://dx.doi.org/10.1021/acs.chemmater.0c00179
Chem. Mater. 2020, 32, 3150−3159

inaccuracy of γ value due to a very difficult measurement process in ref 26.

In the previous report on superconductivity in LiBi[14] the Li isotope effect was studied. Replacing natural abundance Li (m_{Li} = 6.94 u) with Li^6 was found to increase the critical temperature by about 0.02 K. This can be used to additionally verify our calculations, the isotope effect experiments were simulated by the appropriate change in the atomic mass of Li, with the results shown in Table 1. The computed critical temperature increased by 0.026 K and taking into account the small absolute values of those increases, the agreement is considered as very good, validating our theoretical results.

CONCLUSIONS

In summary, we have grown single crystals of LiBi, which contains the lightest and the heaviest nonradioactive metallic elements together. This compound forms in a tetragonal (CuAu-type) crystal structure with Bi square planes separated by Li planes. The distortion from an ideal cubic CsCl structure, yielding c/a = 1.26, is rather large. Due to this distortion, which we argue is driven by the lower energy of a structure that reduces the degeneracy of the p_z orbitals from the p_x and p_y orbitals of Bi, a quasi-two-dimensional character of the electronic structure is seen in both Fermi surface shape and charge density distribution, where metallic Bismuth layers are separated by Lithium planes.

Detailed experimental and theoretical studies of the superconducting and normal state parameters for LiBi are presented. We find LiBi to be a moderately coupled type-I superconductor with T_c = 2.48 K and a critical field $H_c(0)$ = 157 Oe. Our calculations show that the electron−phonon coupling is strongest for the acoustic phonons (Bi vibrations), with, importantly, an additional (15% of the total λ_{e-p}) contribution from Li modes, which is responsible for the larger T_c of LiBi, compared to NaBi. As Bismuth atoms provide majority of both the electronic states at the Fermi surface and phonons for the electron−phonon coupling, we conclude that the Bi square net is responsible for superconductivity of LiBi, but that the coupling between the light element planes and the heavy element planes makes a significant contribution to the superconductivity. As this compound is electronically dominated by Bi square planes with partly filled p orbitals separated by the lightest possible metallic element Li, it offers a unique opportunity to study the superconductivity of Bi square planes using various spectroscopic methods, thus studies like ARPES should be of future interest.

MATERIALS AND METHODS

Single crystals of LiBi were grown by the flux method, using Bi flux. Elemental Li pieces (99.9%, Alfa Aesar) and Bi shot (99.99%, Alfa Aesar) in an atomic ratio 1:2 were packed in a niobium crucible, covered with a plug of quartz wool and sealed inside a silica tube under a partial pressure of Ar. Complete sample preparation was performed in an Ar-filled glovebox without exposing the Li metal to air. The ampule was heated to 500 °C at a rate of 100 °C/h and kept at that temperature for 6 h. After cooling at a rate of 5 °C/h to 270 °C, shiny crystals were separated by decanting the excess of Bi flux using a centrifuge.

The crystal structure of the sample was determined by the LeBail refinement of room-temperature powder X-ray diffraction (pXRD) data for crushed single crystals collected on a Bruker D8 Advance Eco diffractometer with Cu Kα radiation and LynxEye-XE detector. The LeBail refinement of the pXRD pattern was performed using the code TOPAS. Magnetic properties were measured using a Quantum Design Dynacool Physical Property Measurement System (PPMS) with a vibrating sample magnetometer (VSM) system in the temperature range of 1.7−3.5 K under various applied magnetic fields. The temperature dependencies of the zero-field-cooled (ZFC) and field-cooled (FC) magnetic susceptibility (defined as dM/dH, where M is the magnetization and H is the applied field strength) were measured in an external magnetic field up to 60 Oe. Furthermore, the magnetic field dependencies of the magnetization were measured at various temperatures in the superconducting state. The heat capacity measurements were carried out using the two-τ time- relaxation method in a PPMS Evercool II system. The data were collected between 1.9 and 300 K at 0 Oe and in magnetic fields up to 50 Oe. The crystal of LiBi was mounted to the measuring stage using Apiezon N grease to ensure good thermal contact.

The electronic band structure was calculated with help of pseudopotential and plane wave method implemented in Quantum Espresso.[37] Ultrasoft pseudopotientals have been chosen,[38] along with the Perdew−Burke−Ernzerhof[39] scheme for exchange-correlation effects. For lithium the scalar-relativistic pseudopotential has been used, while for bismuth, the fully relativistic pseudopotential has been chosen because relativistic effects, including spin−orbit coupling (SOC), may be essential for such a heavy element.

The phonons and electron−phonon coupling are calculated with help of density functional perturbation theory (DFPT) as implemented in Quantum Espresso. Phonons were calculated on the mesh of 6 × 6 × 6 q points on the basis of the band structure calculated on the mesh of 18 × 18 × 18 k points. Electron−phonon coupling was obtained on the basis of the phonons, and the band structure calculated on a mesh of 36 × 36 × 36 k points.

ASSOCIATED CONTENT

Supporting Information

The Supporting Information is available free of charge at https://pubs.acs.org/doi/10.1021/acs.chemmater.0c00179.

Powder X-ray diffraction pattern of LiBi; the SEM image of LiBi single crystal; structure of KBi featuring Bi spiral chains; electronic structure of LiBi calculated in scalar- and fully relativistic way; phonon structure and electron−phonon coupling in NaBi; the phonon displacement patterns of the six phonon modes for q = (0,0,0.5) of LiBi (PDF)

AUTHOR INFORMATION

Corresponding Author

Tomasz Klimczuk − *Faculty of Applied Physics and Mathematics and Advanced Materials Centre, Gdansk University of Technology, 80-233 Gdańsk, Poland;* orcid.org/0000-0002-7089-4631; Email: tomasz.klimczuk@pg.edu.pl

Authors

Karolina Górnicka − *Faculty of Applied Physics and Mathematics and Advanced Materials Centre, Gdansk University of Technology, 80-233 Gdańsk, Poland*

Sylwia Gutowska − *Faculty of Physics and Applied Computer Science, AGH University of Science and Technology, 30-059 Kraków, Poland*

Michał J. Winiarski − *Faculty of Applied Physics and Mathematics and Advanced Materials Centre, Gdansk University of Technology, 80-233 Gdańsk, Poland;* orcid.org/0000-0001-9083-8066

Bartlomiej Wiendlocha − *Faculty of Physics and Applied Computer Science, AGH University of Science and Technology, 30-059 Kraków, Poland*

https://dx.doi.org/10.1021/acs.chemmater.0c00179
Chem. Mater. 2020, 32, 3150−3159

Weiwei Xie − *Department of Chemistry, Louisiana State University, Baton Rouge, Louisiana 70803, United States;* orcid.org/0000-0002-5500-8195

R. J. Cava − *Department of Chemistry, Princeton University, Princeton, New Jersey 08544, United States*

Complete contact information is available at: https://pubs.acs.org/10.1021/acs.chemmater.0c00179

Notes

The authors declare no competing financial interest.

■ ACKNOWLEDGMENTS

The research performed at the Gdansk University of Technology was supported by the National Science Centre (Poland) grant (UMO-2017/27/B/ST5/03044). The synthesis and magnetic properties measurements performed at Princeton were supported by the Department of Energy, Division of Basic Energy Sciences, grant DEFG02-98ER45706. W.X. is supported by the Beckman Young Investigator (BYI) Program. The research performed at the AGH-UST was supported by the National Science Center (Poland), Project No. 2017/26/E/ST3/00119. S.G. was partly supported by the EU Project POWR.03.02.00-00-I004/16.

■ REFERENCES

(1) Tremel, W.; Hoffmann, R. Square Nets of Main-Group Elements in Solid-State Materials. *J. Am. Chem. Soc.* **1987**, *109* (1), 124−140.

(2) A. Papoian, G.; Hoffmann, R. Hypervalent Bonding in One, Two, and Three Dimensions: Extending the Zintl-Klemm Concept to Nonclassical Electron-Rich Networks. *Angew. Chem., Int. Ed.* **2000**, *39* (14), 2408−2448.

(3) de Marcillac, P.; Coron, N.; Dambier, G.; Leblanc, J.; Moalic, J.-P. Experimental Detection of α-Particles from the Radioactive Decay of Natural Bismuth. *Nature* **2003**, *422* (6934), 876−878.

(4) Mizoguchi, H.; Matsuishi, S.; Hirano, M.; Tachibana, M.; Takayama-Muromachi, E.; Kawaji, H.; Hosono, H. Coexistence of Light and Heavy Carriers Associated with Superconductivity and Antiferromagnetism in CeNi 0.8 Bi 2 with a Bi Square Net. *Phys. Rev. Lett.* **2011**, *106* (5). DOI: 10.1103/PhysRevLett.106.057002.

(5) Han, F.; Malliakas, C. D.; Stoumpos, C. C.; Sturza, M.; Claus, H.; Chung, D. Y.; Kanatzidis, M. G. Superconductivity and Strong Intrinsic Defects in LaPd 1 − x Bi 2. *Phys. Rev. B: Condens. Matter Mater. Phys.* **2013**, *88* (14). DOI: 10.1103/PhysRevB.88.144511.

(6) Park, J.; Lee, G.; Wolff-Fabris, F.; Koh, Y. Y.; Eom, M. J.; Kim, Y. K.; Farhan, M. A.; Jo, Y. J.; Kim, C.; Shim, J. H.; et al. Anisotropic Dirac Fermions in a Bi Square Net of SrMnBi 2. *Phys. Rev. Lett.* **2011**, *107* (12). DOI: 10.1103/PhysRevLett.107.126402.

(7) Sei, R.; Kitani, S.; Fukumura, T.; Kawaji, H.; Hasegawa, T. Two-Dimensional Superconductivity Emerged at Monatomic Bi $^{2-}$ Square Net in Layered Y $_2$ O $_2$ Bi via Oxygen Incorporation. *J. Am. Chem. Soc.* **2016**, *138* (35), 11085−11088.

(8) Winiarski, M. J.; Wiendlocha, B.; Gołąb, S.; Kushwaha, S. K.; Wiśniewski, P.; Kaczorowski, D.; Thompson, J. D.; Cava, R. J.; Klimczuk, T. Superconductivity in CaBi $_2$. *Phys. Chem. Chem. Phys.* **2016**, *18* (31), 21737−21745.

(9) Dshemuchadse, J.; Steurer, W. Some Statistics on Intermetallic Compounds. *Inorg. Chem.* **2015**, *54* (3), 1120−1128.

(10) Zintl, E.; Brauer, G. Konstitution Der Lithium-Wismut-Legierungen: 14. Mitteilung Über Metalle u. Legierungen. *Z. Für Elektrochem. Angew. Phys. Chem.* **1935**, *41* (5), 297−303.

(11) Zintl, E.; Dullenkopf, W. Metals and Alloys. III. Polyantimonides, Polybismuthides and Their Transformation into Alloys.; *Z. Phys. Chem.*, **1932**; Vol. *16*. DOI: 10.1515/zpch-1932-1615

(12) Emmerling, F.; Längin, N.; Petri, D.; Kroeker, M.; Röhr, C. Alkalimetallbismutide ABi und ABi2 (A= K, Rb, Cs)— Synthesen, Kristallstrukturen, Eigenschaften. *Z. Anorg. Allg. Chem.* **2004**, *630* (1), 171−178.

(13) Alekseevskii, N. E.; Brandt, N. B.; Kostina, T. I. Superconductivity of Binary Alloys of Bismuth; 233-63; *Izv. Akad. Nauk SSSR Ser. Fiz*, 1952; Vol. *16*.

(14) Sambongi, T. Superconductivity of LiBi. *J. Phys. Soc. Jpn.* **1971**, *30* (1), 294−294.

(15) Massalski, T. B. Binary Alloy Phase Diagrams. *ASM Int.* **1992**, *3*, 2874.

(16) Xu, Y.; Yamazaki, M.; Villars, P. Inorganic Materials Database for Exploring the Nature of Material. *Jpn. J. Appl. Phys.* **2011**, *50* (11), 11RH02.

(17) Nesper, R. Structure and Chemical Bonding in Zintl-Phases Containing Lithium. *Prog. Solid State Chem.* **1990**, *20* (1), 1−45.

(18) Min, B. I.; Shim, J. H.; Park, M. S.; Kim, K.; Kwon, S. K.; Youn, S. J. Origin of the Stabilized Simple-Cubic Structure in Polonium: Spin-Orbit Interaction versus Peierls Instability. *Phys. Rev. B: Condens. Matter Mater. Phys.* **2006**, *73* (13), 132102.

(19) Zalkin, A.; Ramsey, W. J. Intermetallic Compounds between Lithium and Lead. IV. The Crystal Structure of Li $_{22}$ Pb $_5$. *J. Phys. Chem.* **1958**, *62* (6), 689−693.

(20) Xie, W.; Luo, H.; Baroudi, K.; Krizan, J. W.; Phelan, B. F.; Cava, R. J. Fragment-Based Design of NbRuB as a New Metal-Rich Boride Superconductor. *Chem. Mater.* **2015**, *27* (4), 1149−1152.

(21) Gui, X.; Sobczak, Z.; Chang, T.-R.; Xu, X.; Huang, A.; Jia, S.; Jeng, H.-T.; Klimczuk, T.; Xie, W. Superconducting SrSnP with Strong Sn−P Antibonding Interaction: Is the Sn Atom Single or Mixed Valent? *Chem. Mater.* **2018**, *30* (17), 6005−6013.

(22) Zhao, L. L.; Lausberg, S.; Kim, H.; Tanatar, M. A.; Brando, M.; Prozorov, R.; Morosan, E. Type-I Superconductivity in $YbSb_2$ Single Crystals. *Phys. Rev. B: Condens. Matter Mater. Phys.* **2012**, *85* (21). DOI: 10.1103/PhysRevB.85.214526.

(23) Sun, S.; Liu, K.; Lei, H. Type-I Superconductivity in KBi_2 single Crystals. *J. Phys.: Condens. Matter* **2016**, *28* (8), 085701.

(24) Svanidze, E.; Morosan, E. Type-I Superconductivity in $ScGa_3$ and $LuGa_3$ Single Crystals. *Phys. Rev. B: Condens. Matter Mater. Phys.* **2012**, *85* (17), 174514.

(25) Peets, D. C.; Cheng, E.; Ying, T.; Kriener, M.; Shen, X.; Li, S.; Feng, D. Type-I Superconductivity in Al 6 Re. *Phys. Rev. B: Condens. Matter Mater. Phys.* **2019**, *99* (14). DOI: 10.1103/PhysRevB.99.144519.

(26) Kushwaha, S. K.; Krizan, J. W.; Xiong, J.; Klimczuk, T.; Gibson, Q. D.; Liang, T.; Ong, N. P.; Cava, R. J. Superconducting Properties and Electronic Structure of NaBi. *J. Phys.: Condens. Matter* **2014**, *26* (21), 212201.

(27) McMillan, W. L. Transition Temperature of Strong-Coupled Superconductors. *Phys. Rev.* **1968**, *167* (2), 331−344.

(28) Barker, J. A. T.; Breen, B. D.; Hanson, R.; Hillier, A. D.; Lees, M. R.; Balakrishnan, G.; Paul, D. M.; Singh, R. P. Superconducting and Normal-State Properties of the Noncentrosymmetric Superconductor ${\mathrm{Re}}_{3}\mathrm{Ta}$. *Phys. Rev. B: Condens. Matter Mater. Phys.* **2018**, *98* (10), 104506.

(29) Amon, A.; Svanidze, E.; Cardoso-Gil, R.; Wilson, M. N.; Rosner, H.; Bobnar, M.; Schnelle, W.; Lynn, J. W.; Gumeniuk, R.; Hennig, C.; et al. Noncentrosymmetric Superconductor BeAu. *Phys. Rev. B: Condens. Matter Mater. Phys.* **2018**, *97* (1), 014501.

(30) Górnicka, K.; Cava, R. J.; Klimczuk, T. The Electronic Characterization of the Cubic Laves-Phase Superconductor CaRh2. *J. Alloys Compd.* **2019**, *793*, 393−399.

(31) Singh, Y.; Niazi, A.; Vannette, M. D.; Prozorov, R.; Johnston, D. C. Superconducting and Normal-State Properties of the Layered Boride Os B 2. *Phys. Rev. B: Condens. Matter Mater. Phys.* **2007**, *76* (21). DOI: 10.1103/PhysRevB.76.214510.

(32) Singh, J.; Jayaraj, A.; Srivastava, D.; Gayen, S.; Thamizhavel, A.; Singh, Y. Possible Multigap Type-I Superconductivity in the Layered Boride RuB 2. *Phys. Rev. B: Condens. Matter Mater. Phys.* **2018**, *97* (5). DOI: 10.1103/PhysRevB.97.054506.

(33) Otero-de-la-Roza, A.; Johnson, E. R.; Luaña, V. Critic2: A Program for Real-Space Analysis of Quantum Chemical Interactions in Solids. *Comput. Phys. Commun.* **2014**, *185* (3), 1007−1018.
(34) Li, R.; Cheng, X.; Xie, Q.; Sun, Y.; Li, D.; Li, Y.; Chen, X.-Q. Topological Metal of NaBi with Ultralow Lattice Thermal Conductivity and Electron-Phonon Superconductivity. *Sci. Rep.* **2015**, *5* (1). DOI: 10.1038/srep08446.
(35) Gołąb, S.; Wiendlocha, B. Electron-Phonon Superconductivity in CaBi 2 and the Role of Spin-Orbit Interaction. *Phys. Rev. B: Condens. Matter Mater. Phys.* **2019**, *99* (10). DOI: 10.1103/PhysRevB.99.104520.
(36) Allen, P. B.; Dynes, R. C. Transition Temperature of Strong-Coupled Superconductors Reanalyzed. *Phys. Rev. B* **1975**, *12* (3), 905−922.
(37) Giannozzi, P.; Baroni, S.; Bonini, N.; Calandra, M.; Car, R.; Cavazzoni, C.; Ceresoli, D.; Chiarotti, G. L.; Cococcioni, M.; Dabo, I.; et al. QUANTUM ESPRESSO: A Modular and Open-Source Software Project for Quantum Simulations of Materials. *J. Phys.: Condens. Matter* **2009**, *21* (39), 395502.
(38) Dal Corso, A. Pseudopotentials Periodic Table: From H to Pu. *Comput. Mater. Sci.* **2014**, *95*, 337−350.
(39) Perdew, J. P.; Burke, K.; Ernzerhof, M. Generalized Gradient Approximation Made Simple. *Phys. Rev. Lett.* **1996**, *77* (18), 3865−3868.

https://dx.doi.org/10.1021/acs.chemmater.0c00179
Chem. Mater. 2020, 32, 3150−3159